Inhomogeneity of Electron Injection Rates in Dye-Sensitized TiO_2: Comparison of the Mesoporous Film and Single Nanoparticle Behavior†

Toby D. M. Bell,‡,|| Cynthia Pagba,§ Mykhaylo Myahkostupov,§ Johan Hofkens,*,‡ and Piotr Piotrowiak*,§

Department of Chemistry, Katholieke Universiteit Leuven, Celestijnenlaan 200F, B-3001 Heverlee, Belgium, and Department of Chemistry, Rutgers University, 73 Warren Street, Newark, New Jersey 07102

Received: June 26, 2006; In Final Form: September 18, 2006

As it has been shown by pump−probe experiments electron injection at the interface between a dye molecule and mesoporous TiO_2 proceeds with rates exceeding 1×10^{13} s^{-1}. However, similar dye−TiO_2 systems exhibit residual dye emission with lifetimes extending into the long nanosecond range. To address this inhomogeneity of injection rates time-correlated single photon counting microscopy was used to compare the emission behavior of dye-sensitized mesoporous films of TiO_2 with that of individual anatase nanoparticles that had undergone extensive dialysis. The sensitized films produce intense residual emission with multiexponential decay components as long as 220 ns. The channels of mesoporous films contain physisorbed and trapped dye, which is the dominant source of the emission. It is likely that the wide range of lifetimes reflects the distribution of mean free paths experienced by the loose dye molecules diffusing within the film prior to undergoing oxidative quenching. In contrast, the intensity of emission from individual nanoparticles from which the loose dye was removed by dialysis is orders of magnitude lower. The lifetimes obtained from such particles are much shorter, with the primary component on a sub-nanosecond time scale. The presence of residual emission with a 230 ps lifetime shows that even on the surfaces of dialyzed nanoparticles there is a fraction of sensitizer molecules that do not inject electrons with the same high rate as is observed in ultrafast pump−probe experiments on films. Since the physisorbed dye was removed from these samples by dialysis, the residual emission is likely to originate from dye molecules bound to surface defects. Unusual collective emission bursts were observed in some of the measurements on sensitized nanoparticles. We attribute this behavior to stimulated emission from individual nanocrystallites.

Introduction

Interfacial electron injection in dye-sensitized TiO_2 mesoporous films continues to receive tremendous attention, primarily because of the potential application of these materials in solar energy conversion. Despite this intense research activity some key fundamental aspects of the "Graetzel cell" remain poorly understood. Among those is the broad inhomogeneity of electron injection rates that are being reported for otherwise similar systems. Ultrafast pump−probe absorption experiments in the visible[1−13] and infrared[14−17] show that the dominant fraction of the injection process occurs on a sub-picosecond scale, yet emission measurements on seemingly identical systems reveal readily detectable dye luminescence with lifetimes extending well into the nanosecond domain.[18−25] Similarly, microwave absorption experiments suggest the presence of a slow charge separation process occurring on a short nanosecond time scale.[26,27] This injection rate inhomogeneity spanning at least 6 orders of magnitude must result from a broad range of dye−semiconductor electronic interactions, which in turn points to a correspondingly broad distribution of dye−substrate binding. To probe the broad distribution of injection rates we used time-correlated single photon counting (TCSPC) microscopy to compare the emission behavior of dye-sensitized mesoporous films of TiO_2 with that of individual anatase nanoparticles that had undergone extensive dialysis. The residual luminescence of the dye detected either in static emission measurements or in TCSPC experiments on sensitized TiO_2 typically accounts for a few percent of the initial excited-state population.[19,20,25] While in early studies the emission decay was frequently interpreted as the true measure of the electron injection rate, the more recent ultrafast experiments show that the bulk of the injection process in the case of Ru-type sensitizers usually exceeds 1×10^{13} s^{-1}. Indeed, there is increasing consensus that a substantial fraction of the electron injection occurs from vibrationally and electronically "hot" states of the photoexcited sensitizer,[1−3] even at large chromophore−semiconductor distances.[10] Consequently, the residual emission is increasingly viewed as the signature of a "bad dye", i.e., dye molecules which upon photoexcitation either inject electrons at an abnormally slow rate or do not undergo electron injection at all. The origin of this behavior is not fully understood. In this paper we attempt to identify the possible sources of the electron injection inhomogeneity by using confocal TCSPC microscopy and comparing the residual emission behavior of dye-sensitized mesoporous films of TiO_2 prepared in the typical "Graetzel cell" fashion with that of individual TiO_2 nanoparticles that had undergone extensive postsensitization dialysis (Figure 1). Second, we would like to narrow the discrepancy between the

† Part of the special issue "Arthur J. Nozik Festschrift".

* Author to whom correspondence should be addressed. Phone: (973) 353-5318. Fax: (973) 353-1264. E-mail: piotr@andromeda.rutgers.edu.

‡ Katholieke Universiteit Leuven.

§ Rutgers University.

|| Present address: School of Chemistry, University of Melbourne, Parkville 3010, Australia.

10.1021/jp064005f CCC: $33.50
Published on Web 10/31/2006

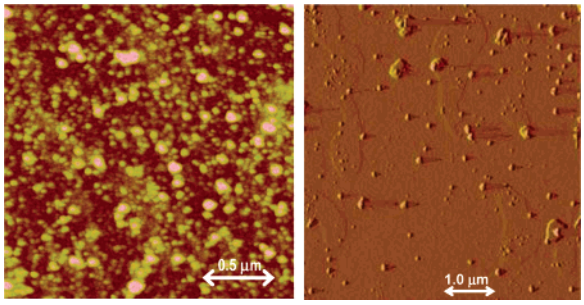

Figure 1. Tapping mode atomic force microscopy images of a continuous mesoporous TiO_2 film (left) and dispersed TiO_2 nanoparticles (right) used in the reported studies. Both samples were prepared from the same batch of TiO_2 to ensure similar crystallinity. Note the presence of individual particles and particle clusters in the image on the right. The surface coverage is ~100 times higher than that employed in the TCSPC confocal microscopy experiments.

electron injection rates obtained using ultrafast pump−probe transient absorption techniques and those deduced from emission quenching kinetics. While the pump−probe experiments offer a more direct measure of the injection rate, emission experiments have the important advantage of being far more sensitive, and hence they are the only approach applicable to the study of interfacial photoinduced processes on individual nanoparticles. The channels of continuous mesoporous films can contain a fraction of loosely bound, primarily physisorbed, and perhaps even simply trapped dye, which is likely to be the dominant source of residual emission. Indeed, many of the effective surface coverage figures reported for sensitized mesoporous films of TiO_2 correspond to amounts of dye that greatly exceed the available surface area and can be explained only if multiple layers of sensitizer are present.[19] Such heterogeneous structures consisting of the covalently bound layer overcoated with layers of physisorbed dye would certainly give rise to a highly inhomogeneous electron injection dynamics.[28] Photoexcitation of dye molecules in the distant physisorbed layers can still lead to electron injection through a combination of exciton hopping followed by the final electron-transfer step. Such a stepwise quenching process will be necessarily slower than direct injection, and its rates will reflect the distance distribution between the excitation site and the surface of the semiconductor. In the case of individual TiO_2 nanoparticles the possibility of dye trapping within the voids is eliminated, and hence the slowest, diffusional component of electron injection should be completely absent. Furthermore, repeated dialysis ought to remove physisorbed dye molecules thus preventing the formation of layered structures on the particle surface. Only the dye molecules that are truly chemically bound to the surface will not be affected by repeated washings and dialysis. Consequently, it was expected that the inhomogeneiety of injection rates should be greatly reduced for individual dialyzed particles and reflect primarily the imperfections of the nanoparticle surface.

Experimental Details

Materials and Sample Preparation. *Continuous Mesoporous Films.* A colloidal solution of TiO_2 was prepared following the modified procedure described by Graetzel et. al.[29] Ten milliliters of titanium isopropoxide was added slowly to 60 mL of distilled water (pH = 1, 70% HNO_3). The mixture was heated (approximately 8 h) at 95 °C until the white precipitate dissolved. The final volume of the solution was adjusted such that the concentration was approximately 160−170 g/L. A 20 mL aliquot was digested at 200 °C for 12 h and cooled to room temperature. The average particle size was determined by light scattering measurements (Wyatt Technology Dawn EOS, with a Wyatt quasi-elastic light scattering detector). For film preparation, 2−3 drops of TiO_2 colloidal solution were deposited on a glass cover slip, spread with a glass rod, and annealed at 450 °C for 30 min. The films were soaked in a 1×10^{-4} M acetonitrile solution of the dye for at least 12 h. The sensitized films were then repeatedly rinsed and soaked in acetonitrile overnight to remove the unbound dye. The ZrO_2 nanoparticles and sensitized films were prepared in an analogous fashion from zirconium isopropoxide.

Dispersed Nanoparticle Samples. Anatase TiO_2 nanoparticles were prepared following the procedure described by Hartland et al.,[13] with slight modifications. A freshly prepared solution of 3 mL of titanium(IV) isopropoxide (Acros, 98+%) and 60 mL of 2-propanol was added slowly (~1 drop s^{-1}) to 300 mL of oxygen-free water (pH = 1, HCl) water at 0 °C under nitrogen and vigorous stirring. The resulting solution was stirred at 0 °C for 3 h and then left overnight (with continuous stirring). The solvent was removed by rotary evaporation. The resulting nanoparticles had an average diameter of 10 nm. For film preparation, a 2×10^{-5} M ethanol solution of the dye was mixed with an equal volume of 100 mg/L colloidal TiO_2 solution. The resulting mixture was dialyzed using a Spectrapor Standard RC membrane (6−8 kD) against deionized distilled water five times. A membrane with a 6−8 kD cutoff is permeable to the dye molecules and small nanoparticles up to ~3 nm in diameter. The thoroughly dialyzed solution was subsequently deposited on the glass cover slip and air-dried at room temperature.

Glass Substrate Pretreatment: The cover glass slips were cleaned by sonicating them consecutively in acetone, 1 M NaOH, and Milli-Q water. They were then soaked in 0.1 M HCl solution for 24 h and dried with nitrogen flow.

Static Absorption and Emission Spectroscopy. Absorption spectra of the sensitized films and colloidal suspensions of nanoparticles were obtained using a Cary 500 UV−vis−near-IR spectrophotometer and a Cary Eclipse fluorimeter. The absorption spectra were collected in standard transmission mode. In the case of the films a fragment of the cover slide with the film was placed in a cuvette filled with the solvent. The slide was normal to the beam in the absorption measurements and angled at 45° in fluorescence experiments

Confocal TCSPC Measurements. Full details of the experimental setup used for the single nanoparticle measurements are published elsewhere.[30] In brief, the second harmonic 488 nm output (1.2 ps full width at half-maximum) of a Ti:sapphire laser (Tsunami, Spectra Physics) was directed into an inverted confocal microscope (Olympus IX 70) equipped with a piezo-controlled scanning stage (Physik Instrumente) and focused onto the sample through an oil immersion objective (Olympus, 100×; 1.4 NA). Luminescence from the sample was collected through the same objective and separated from the excitation light with a series of dichroic, notch, and band-pass filters. One-half of the emission was directed onto an avalanche photodiode (SPAD-SPCM 15 EG&G), and the other half onto a liquid nitrogen cooled CCD camera (Princeton Instruments). Sample images were acquired via raster scanning with a dwell time of 1 ms, fluorescence spectra via the CCD camera coupled to a polychromator, and fluorescence trajectories via the APD and a TCSPC card (SPC 630, PicoQuant) operating in "first in first out" (FIFO) mode. The measurements were performed in ambient atmosphere. Each photon emitted has its chronological time stamp as well as its timing with respect to the excitation pulse recorded. These data allow the generation of time-resolved

decay histograms along the trajectories, which were analyzed using a homemade program based on the Maximum Likelihood Estimator.[31]

Pump−Probe Transient Absorption Experiments. Pump−probe transient absorption measurements were performed using two noncollinear optical parametric amplifiers (NOPAs, TOPAS-White and TOPAS-White IR, both by Light Conversion, Inc.). One of the NOPAs was tuned to 520 nm and served as the excitation source, while the idler of the other was tuned to near IR wavelengths in the 900−1300 nm range and served as the probe source. The energy of the excitation pulse was <10 μJ, and that of the probe pulse <2 μJ. The beams were guided by all-reflective optics (Al and Au) and crossed at an angle of ~10° at the sample well ahead of the focal point of the final Al off-axis parabolic mirror, with an approximate spot size at the sample of 0.5 mm. Both NOPAs were pumped by a home-built multipass Ti:sapphire amplifier operating at 1.25 kHz. The amplifier was seeded by a Spectra Physics Tsunami mode-locked oscillator and pumped by a Quantronix Falcon frequency-doubled Nd:YLF laser. The pulse injection was accomplished using a FastPulse Pockels cell and driver. The synchronization between the seed laser and the multipass amplifier was provided by a Stanford Research Systems DG535 pulse and delay generator in conjunction with frequency divider modules (Pulse Research Laboratories). The all-reflective pulse stretcher and compressor were purchased from the Kapteyn & Murnane Laboratories. The delay between the pump and probe pulses was varied using a Newport translation stage with 0.1 μm (0.67 fs) resolution that was controlled using a LabView subroutine. The data were collected using either a Si or a Ge photodiode (both from Thorlabs) and a digital lock-in amplifier (Stanford Research Systems, SR810) with an amplitude modulation frequency of 17 Hz (New Focus Optical Chopper 3501). The sample (sensitized TiO_2 film on a 0.17 mm microscope cover glass) was placed in a gentle flow of N_2 gas to minimize the photobleaching effects.

Nanosecond Emission and Absorption Measurements. Emission lifetimes of $Ru(bpy)_2(dcbpy)^{2+}$ in solution were determined using the second harmonic of a Q-switched Nd:YAG laser (Quantel Brilliant II) as the excitation source and a Hamamatsu R928 photomultiplier tube as the detector. The detection wavelength was selected using an Oriel MS257 monochromator. The liquid samples were degassed by four freeze−pump−thaw cycles. The emission lifetimes of the dye on insulating ZrO_2 films were measured in ambient atmosphere. Excited-state lifetimes were also measured in the absorption mode using the same experimental setup with a Hamamatsu xenon flashlamp serving as the source of the probe light.

Results and Discussion

The dye selected for this study was, bis(2,2′-bipyridine)(4,4′-dicarboxy-2,2′-bipyridine)ruthenium(II), abbreviated as $Ru(bpy)_2(dcbpy)^{2+}$, which in addition to being one of the most ubiquitous TiO_2 sensitizers has the advantage of having a much higher photochemical and photoredox stability than that of most organic dyes. It is believed that the presence of carboxylic or phosphonate groups is necessary to bind the dye tightly to the metal oxide surface. The precise nature of the surface bond is still being disputed, with some IR and Raman spectroscopy experimental evidence supporting the formation of stable ester linkages and other evidence pointing to direct coordination of the Ti centers, in either a bridging or a chelating mode.[32,33] While the acidic functional groups ensure the stability of binding, it is not certain whether they are indispensable for rapid interfacial electron injection.[34] The closely related $Ru(dcbpy)_3^{2+}$ dye bearing two carboxylic groups on each bipyridine ligand has been used in a highly efficient regenerative solar cell based on the Br_2/Br^- redox couple, which exhibited a monochromatic light to power conversion efficiency of 12% at the wavelength of maximum absorption. While the spectral response of the more recently developed Ru^{II} dyes has been significantly improved, this power conversion efficiency remains among the highest. The number of turnovers exceeded 10^4, indicating that the quantum yield of the side reactions was lower than 10^{-5}. The incident photon to current efficiencies (IPCEs) of the device reached 73%, suggesting that a substantial fraction of the dye did not undergo electron injection. It was decided to chose the dicarboxy $Ru(bpy)_2(dcbpy)^{2+}$ dye rather than the $Ru(dcbpy)_3^{2+}$ for the present study because the six peripheral carboxylic groups of the latter enable binding to multiple nanoparticles and induce pronounced aggregation of TiO_2.[20] Minimizing TiO_2 aggregation was crucial for the extended dialysis treatment of sensitized nanoparticles and for the single nanoparticle microscopy experiments. After TiO_2 binding the absorption spectrum of $Ru(bpy)_2(dcbpy)^{2+}$ becomes broadened and red-shifted, with the λ_{max} of 469 nm in a colloidal suspension and 460 nm in a mesoporous film, compared with 454 nm in a homogeneous ethanolic solution (Figure 2a). In a well-degassed CH_3CN solution the measured single-exponential emission lifetime of the $Ru(bpy)_2(dcbpy)^{2+}$ metal-to-ligand charge transfer (MLCT) state is 490 ns. This is consistent with the 0.5 μs reported in the literature for degassed aqueous solutions.[25] It was observed by the same group that the lifetime of the excited state is lowered to 230 ns upon binding to Al_2O_3 nanoparticles, whose band gap is too large for electron injection to occur.[25] In fully aerated but otherwise identical CH_3CN solution the single-exponential emission lifetime is reduced to 180 ns (Figure 2b). The emission maximum shifts from 619 nm in solution to 636 nm in a mesoporous film TiO_2. There is no appreciable broadening of the dye's emission spectrum upon binding to the film. Even after the film was soaked overnight and rinsed in acetonitrile the residual emission of the sensitized film remains high at approximately 20%, a result that is qualitatively consistent with the 73% IPCE observed by Vlachopoulos et al. for $Ru(dcbpy)_3^{2+}$.[20] These emission yields were compared with the behavior of $Ru(bpy)_2(dcbpy)^{2+}$ bound to a mesoporous ZrO_2 film. The conduction band of ZrO_2 lies too high for electron injection from the MLCT excited states of $Ru(bpy)_3^{2+}$-type dyes, and as a consequence this material is frequently used as a convenient insulating reference substrate. Upon ZrO_2 film binding the emission decay of the dye in ambient atmosphere becomes biexponential, with components $\tau_1 = 46$ ns and $\tau_2 = 320$ of nearly equal amplitudes, $A_1 = 0.54$ and $A_2 = 0.46$, respectively. The presence of the slower component can be ascribed to the restricted oxygen diffusion in the mesoporous medium. The origin of the faster component on a substrate that cannot promote injection is not clear. The static emission yield under continuous irradiation normalized for the absorbance at the excitation wavelength is within few percent of that measured in an aerated solution of $Ru(bpy)_2(dcbpy)^{2+}$ and consistent with the amplitudes of the slow and fast components obtained in the time-resolved measurements.

The first type of sample used in the time-resolved fluorescence microscopy investigation was a continuous, approximately 5-μm-thick anatase film deposited on a thin glass substrate that has been subsequently sensitized by treatment with a solution of $Ru(bpy)_2(dcbpy)^{2+}$ and soaked for 24 h in acetonitrile, a typical procedure that presumably removes the excess unbound

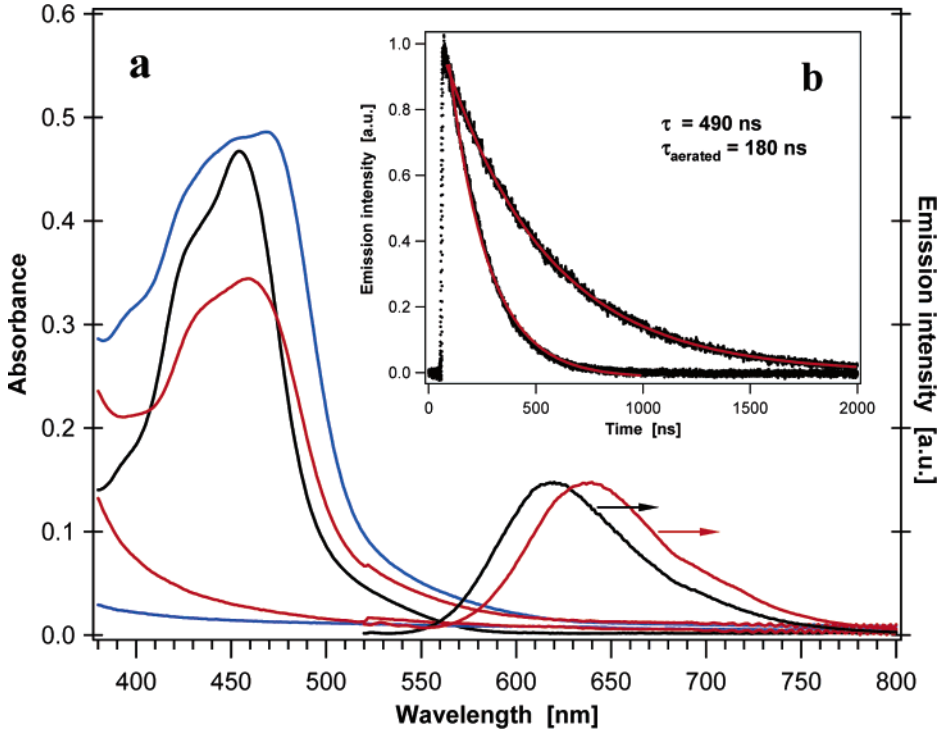

Figure 2. (a) Absorption and emission spectra of $Ru(bpy)_2(dcbpy)^{2+}$ in solution and on TiO_2: black, 50 μM $Ru(bpy)_2(dcbpy)Cl_2$ in EtOH; red, sensitized and blank TiO_2; blue, 1:1 v/v mixture of 100 μM $Ru(bpy)_2(dcbpy)Cl_2$ and 500 mg/L colloidal anatase in EtOH. The spectra of unsensitized film and colloidal TiO_2 are shown for comparison. The absorption spectra were collected in the standard transmission mode and were not corrected for scattering. The emission spectra were normalized to emphasize the bathochromic shift of the dye upon binding on TiO_2. **(b)** Single-exponential emission lifetimes of the MLCT* state of $Ru(bpy)_2(dcbpy)^{2+}$ in degassed and aerated CH_3CN solutions monitored at 600 nm, $\tau = 490$ ns, $\tau_{aerated} = 180$ ns, and $\lambda^{exc} = 532$ nm. The intensities of the traces were normalized.

dye. Our initial pump−probe measurements on sensitized films prepared in this manner yielded a nearly step function response indicating that the bulk of the injection process is completed within the duration of the 100 fs excitation pulse. These results were clearly limited by the ~140 fs cross-corelation of the available pump and probe pulses. New results obtained with a dual NOPA system reveal complex multiexponential electron injection with a dominant 54 fs component (Figure 3 and Table 1). Like others, we assign the fastest ~50 fs component to the injection from the unrelaxed, vibrationally hot, singlet state and the 0.8 ps component to the injection from the triplet state. At long wavelengths, $\lambda > 800$ nm, the transient absorption originates primarily from the singlet and triplet MLCT states of the dye, $Ru(bpy)_2(dcbpy)^{2+}$, and from the electron in the conduction band of TiO_2.[35,36] This behavior, i.e., the dominant fraction of the electron injection occurring within ~100 fs, has been observed for related Ru^{II}-based sensitizers in several laboratories.[2−4,7,8] The slower processes are most likely due to the imperfectly bound dye, and this is the portion of the dye that contributes the most to the residual emission from the sensitized film.

In confocal microscopy experiments photoexcitation of a mesoporous sensitized film that was prepared in an identical fashion produces a strong, characteristic $Ru^{II}(bpy)_3^{2+}$ emission spectrum that undergoes multiexponential decay on a nanosecond time scale (Figure 4a and Table 1). The emission intensity and decay characteristics are uniform across the sampled film area, except for the defective spot that can be seen in the lower left corner of the image in Figure 4a (in the false color image blue corresponds to high intensity, and red to low intensity).

Indeed, confocal fluorescence microscopy appears to be an excellent method for evaluating the quality and consistency of the film preparation and sensitization. The films used in this

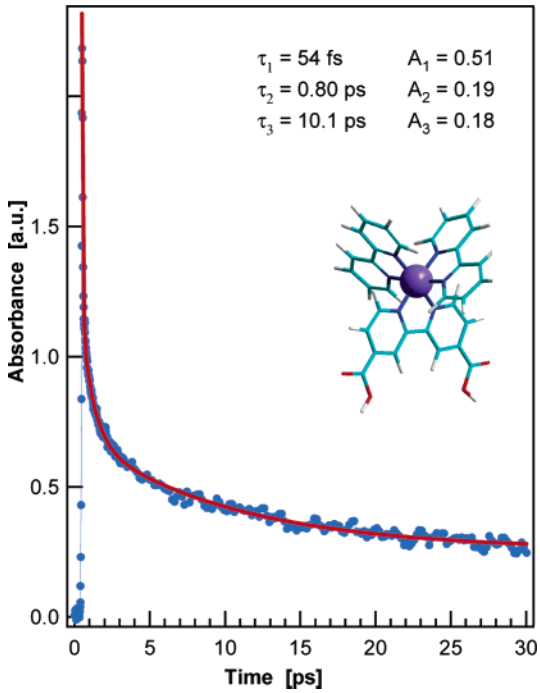

Figure 3. Pump−probe absorption signature of photoinduced electron injection from $Ru(bpy)_2(dcbpy)^{2+}$ into TiO_2 (anatase) mesoporous film, with excitation at 520 nm, monitored at 1000 nm, and an approximate pump−probe cross-correlation of 30 fs. The injection is multiexponential, with the fastest resolved component of 54 fs, followed by a second one of 800 fs. More than 70% of the injection occurs on a sub-picosecond time scale.

study contained very few defects as the one shown in Figure 4a. The complex emission decay is reproduced well by a triple exponential with rates of 20, 72, and 220 ns. Presence of such

TABLE 1: Summary of the Multiexponential Electron Injection Kinetics at the $Ru(bpy)_2(dcbpy)^{2+}/TiO_2$ Interface Obtained in TCSPC Microscopy and Pump−Probe Transient Absorption Experiments

sample type	λ^{meas} (nm)	λ^{exc} (nm)	τ_1 (ns)	A_1	τ_2 (ns)	A_2	τ_3 (ns)	A_3
degassed EtOH solution	600	532	490	1.00				
aerated EtOH solution	600	532	180	1.00				
sensitized ZrO_2 film	600	532	46	0.55	320	0.45		
sensitized film, fs pump−probe	900	520	5.4×10^{-5}	0.51	8.0×10^{-4}	0.19	1.0×10^{-2}	0.18
sensitized film, TCSPC	625	488	20	0.27	72	0.43	220	0.30
sensitized nanoparticles dialyzed 5×	625	488	0.23	0.75	1.7	0.22	8.2	0.03
sensitized nanoparticles dialyzed 2×, early	625	488	1.4	0.74	36	0.26		
sensitized nanoparticles dialyzed 2×, late	660	488	1.3	0.87	32	0.13		
sensitized nanoparticles dialyzed 2×, burst	660	488	1.6	0.97	26	0.03		

slow decay rates is impossible to detect in femtosecond pump−probe experiments, especially if they account only for a few percent of the overall response. The slowest, $\tau = 220$ ns component is only approximately 2 times shorter than the lifetime measured in a well-degassed solution (vide supra). More interestingly, it is *slower* than the 180 ns lifetime obtained in an aerated solution of $Ru(bpy)_2(dcbpy)^{2+}$. This strongly suggests that in mesoporous TiO_2 films there is a fraction of the dye that is sequestered within the interstitial space of the film and undergoes very slow quenching, most likely due to free diffusion in the remaining, similarly trapped solvent. Since the TCSPC microscopy experiments were performed in ambient atmosphere this result suggests that the O_2 quenching of the trapped dye is also impeded due to restricted diffusions within the pores of the film. This slowest component integrated over its lifetime accounts for nearly 70% of the overall detected emission. The faster quenching components may correspond to dye molecules experiencing stronger interaction with the semiconductor substrate. Nevertheless, they are still more than 5 orders of magnitude slower than the injection rate measured in pump−probe experiments (Figure 3). It is plausible that all fitted components originate from diffusional quenching and are linked to the pore size distribution, with their rates reflecting the mean free path traversed between the photoexcitation and the encounter with the wall of the pore.

The behavior of dye-sensitized particles that were dialyzed five times prior to deposition on the glass substrate is dramatically different. The emission spectrum collected from individual dialyzed nanoparticles or nanoparticle clusters is much weaker and consists of the $Ru^{II}(bpy)_3$ component superimposed on a broad background that was present also in unsensitized TiO_2 samples. The luminescence decay kinetics is also entirely different with the rates of primary components falling in the range from 1×10^{10} to 1×10^9 s^{-1} (Table 1). For example, residual emission from a large, 1.2 μm radius particle, shown in Figure 4b has decays of $\tau_1 = 0.23$ ns and $\tau_2 = 1.6$ ns, respectively. The slowest fitted component is now 8.2 ns, and it accounts for only 3% of the overall amplitude. However, integrated over its lifetime it represents a substantial 30% of the total emission yield. Since all trapped and physisorbed dye should have been thoroughly removed by the repeated dialysis, we conclude that the residual emission from individual nanoparticles originates from the dye that is covalently bound to the surface of TiO_2. The fastest, 230 ps component of the emission decay is still 3 orders of magnitude slower than the injection rates obtained from pump−probe experiments on continuous films.

It should be emphasized that all measurements reported in this paper are "single nanoparticle−many molecules" rather than "single nanoparticle−single molecule"[37] or "single molecule−continuous film"[38] experiments, examples of either of which have been reported in the literature. Assuming complete surface coverage, it can be estimated that a 10 nm diameter nanoparticle is coated with approximately 100 $Ru(bpy)_2(dcbpy)^{2+}$ molecules. In the case of a 1 μm particle this number increases to 1×10^6 dye molecules. As a consequence, ensemble behavior was observed for all probed particles, regardless of their size. Since the resolution of a confocal microscope can at best approach the diffraction limit, the size of the nanoparticle can be resolved only if its diameter is larger than the waist of the laser beam at the focus of the objective. This means that the images of all particles smaller than ~300 nm appear to be of the same size, with only the intensity of emission giving a hint of their relative dimensions.

The overall yields of residual emission of continuous film and dialyzed particles can be compared only in an approximate manner, since it is difficult to quantitatively evaluate the absorbance cross-sections of individual particles with a broad size distribution, ranging from radii much smaller to larger than the radius of the excitation beam at the focus of the microscope. Nevertheless, it can be very conservatively estimated that the residual emission from individual nanoparticles is diminished by more than two orders of magnitude in comparison with continuous mesoporous films. As a consequence, it is safe to conclude that more than 99% of emission measured from Ru-type dye-sensitized mesoporous TiO_2 films originates from dye molecules that are not covalently bound to the semiconductor surface. Correspondingly, only a negligible fraction, less than 0.1% of the covalently bound dye, undergoes electron injection sufficiently slowly to produce the observed emission. The nature of this small dye population remains difficult to ascertain. Binding to surface defects can lead to less favorable electronic interactions and reduce the thermodynamic driving force for electron injection. Several studies point to a strong link between the TiO_2 crystallinity and the efficacy of electron injection as well as the distribution of recombination rates;[5,11] however, even the most carefully prepared and characterized TiO_2 nanoparticles result in broadly inhomogeneous interfacial electron-transfer kinetics. The TiO_2 preparation procedure adopted in this work is known to lead to crystalline anatase particles,[13] as was confirmed on selected batches by transmission electron microscopy and Raman spectroscopy. The crystallinity of the nanoparticles after the dialysis treatment was not tested.

All measurements described in this paper were performed in ambient atmosphere without any provisions to protect the samples from contact with air. Progressive oxidative photodegradation of all samples was observed, as reported earlier.[35] The photodamage was least pronounced for the continuous TiO_2 films. It was most rapid for small nanoparticles, in which case total disappearance of the dye emission was observed after less than a minute of low-power irradiation (Figure 5). Interestingly, the photodestruction of the dye does not eliminate all emission from the sample. A broad, short-lived photoluminescence stretching from 550 to 820 nm remains present regardless of

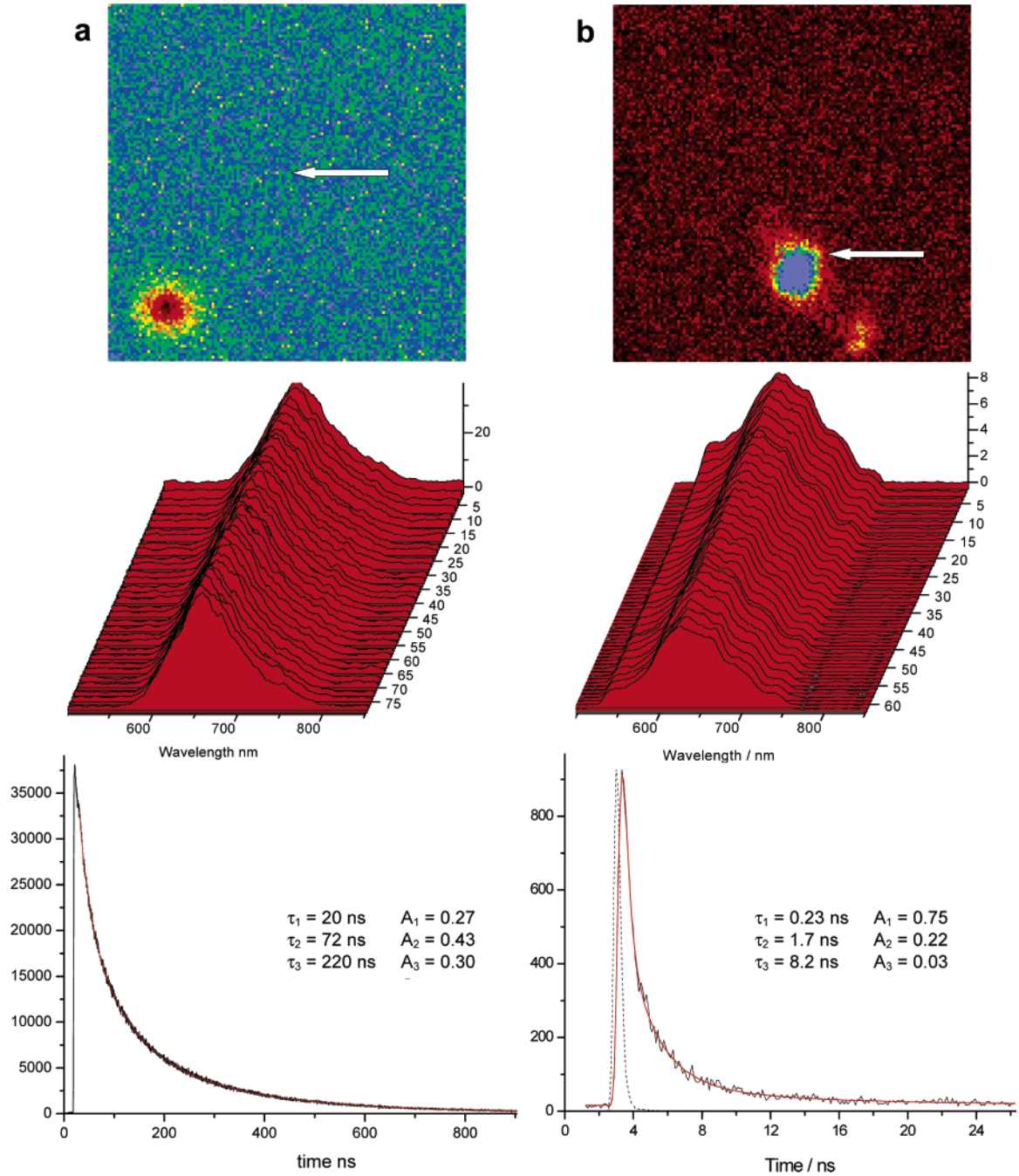

Figure 4. Emission quenching kinetics and spectral evolution of $Ru(bpy)_2(dcbpy)^{2+}$ on TiO_2 surfaces: **(a)** Uniformly coated continuous mesoporous film, 30 × 30 μm^2 image size. Spectra and decays collected simultaneously in confocal mode from the area indicated by the arrow. Blue pixels correspond to high emission intensity, and red to low intensity. Spectra were collected every 3 s. The prominent dark red area in the lower left is a defect in the film. **(b)** Individual dye-sensitized particles treated by 5-fold dialysis prior to deposition on the substrate, 20 × 20 μm^2. Spectra and decays were collected simultaneously in confocal mode from the area indicated by the arrow. Spectra were collected every 4 s. Note the different time scales of the decay profiles in Figures 4a and 4b.

the length of irradiation. The spectrum of this residual emission most likely originates from the decomposition products and is different from that observed for untreated TiO_2 samples, with the maximum at 660 versus 560 nm. It is also possible that a fraction of the decrease of emission upon prolonged irradiation is due to sample annealing. Some of the imperfectly bound "bad dye" molecules could become better (faster) electron injectors upon local heating and emit fewer photons.

As mentioned earlier, all sampled particles exhibited ensemble behavior, consistent with the presence of multiple dye molecules on the surfaces of even the smallest nanoparticles. A typical trajectory, in this case obtained from a nanoparticle after 2-fold dialysis, is shown in Figure 6a below. It can be seen that its main feature is the gradual decrease of the photon count due to photodamage. However, a prominent burst of the number of detected photons is visible after 345 s of irradiation. The amplitude of the burst is 4-fold higher than the preceding sections of the trajectory. It clearly exceeds the random fluctuations and indicates a collective event of unknown nature. The photon burst has a distinct decay signature, different from the transients collected before and after its occurrence. The slow component of the fitted double exponential that accounts for an appreciable fraction of the emission intensity during most of the time scan is nearly completely absent during the burst (Table 1). Indeed, the decay within the burst is the closest to a homogeneous single-exponential behavior that was observed in

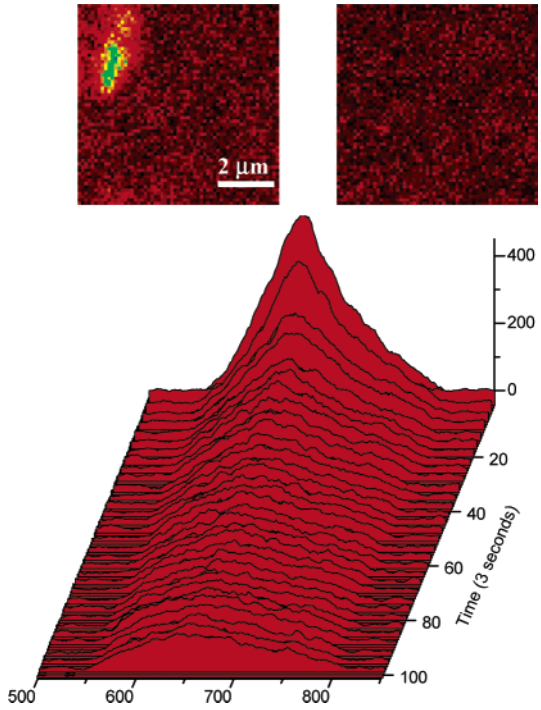

Figure 5. Spectral evolution of a small, spatially resolved, cluster of dye-sensitized nanoparticles (the bright green area in the upper left corner the first image) upon continuous irradiation. The initial emission of the Ru dye is replaced by a broad, short-lived background. After approximately 60 s of irradiation the dye emission disappears completely (the second image of the same 7×7 μm^2 area shown on the right). Spectra were collected at 3 s intervals.

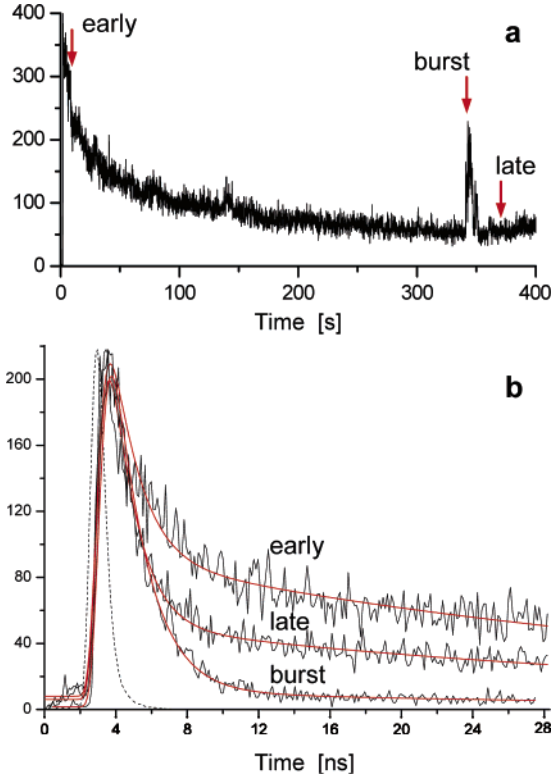

Figure 6. (a) Photon counting trajectory of the sample in Figure 3. The system exhibits ensemble behavior with pronounced bleaching. An intense burst of emitted photons occurs at approximately 345 s. A smaller burst is visible at 140 s. **(**b**)** Normalized decays and double-exponential fits of the following sections of the trajectory: (i) early, from 2.0 to 8.0 s, $\tau_1 = 1.4$ ns, $A_1 = 0.74$, $\tau_2 = 36$ ns, $A_2 = 0.26$; (ii) late, from 355 to 385 s, $\tau_1 = 1.3$ ns, $A_1 = 0.87$, $\tau_2 = 32$ ns, $A_2 = 0.13$; (iii) the burst, $\tau_1 = 1.6$ ns, $A_1 = 0.97$, $\tau_2 = 26$ ns, $A_2 = 0.03$. The instrumental response function is shown with the dotted line.

this entire study. Similar but smaller bursts and "dips" were observed in several other trajectories of small particles, pointing to a collective response of several (many) dye molecules. The burst persists for several seconds, i.e., for a large number of excitation cycles. We cannot offer a fully satisfactory explanation of this behavior. It is possible that the bursts are due to stimulated emission that could occur as a result of fluctuations in the pump beam intensity and mode. Stimulated emission and low-threshold lasing from dye-doped TiO_2 microcrystallites[39] and liquid microdroplets[40,41] acting as resonant cavities have been observed in several studies. The short, homogeneous emission lifetime observed during the bursts reported here is consistent with this hypothesis. It has been shown that the onset of the microcavity lasing is extremely sensitive to the excitation intensity and beam coupling parameters,[42,43] which in our work can be influenced by local heating and bleaching effects.

It should be noted that the presented single particle measurements are inherently biased toward larger particles and particle clusters, which are more prone to be polycrystalline and to contain defects. First, the dialysis stage removes not only the loosely bound dye but also the smaller and hence presumably more perfect nanoparticles that can permeate through the pores of the membrane. Second, it is a natural tendency in the confocal emission experiments to select the brighter and therefore larger particles. Indeed, on the basis of the intensity alone it is impossible to distinguish the brighter or simply larger particles unless their size exceeds the confocal limit of $\sim\lambda/2$. In our measurements we examined both large and small particles, although the sampling certainly falls well short of being statistical. Their spectral and dynamic behaviors were very similar, except for the photobleaching rate, which was much faster for the smaller (less bright) particles (vide infra). The spectra always consisted of the Ru dye component superimposed on the background, and the triple-exponential fits always yielded rates in the sub-nanosecond to short nanosecond range.

With the above caveat in mind, it should be pointed out that the true "single molecule−single nanoparticle" experiments that have been attempted on sensitized TiO_2 nanoparticles are subject to a much heavier inherent bias toward the noninjecting dye molecules, as these are the emitters that can be readily detected. Considering that the injection kinetics is highly nonexponential and that the rate of the dominant quenching component exceeds the excited-state lifetime of the dye by approximately 5 orders of magnitude, it is extremely difficult, if at all possible, to select a representative dye−nanoparticle combination in a "single molecule−single nanoparticle" experiment. Depending on the oscillator strength, the probability that an individual surface-bound sensitizer molecule undergoing electron injection within 100 fs will emit a photon is less than 1×10^{-4} for organic laser dyes and less than 1×10^{-6} for $Ru^{II}(bpy)_3$-type dyes, making them a very challenging target for single molecule experiments. Indeed, the recently reported injection rates for the "single coumarin 343 molecule−single TiO_2 nanoparticle" system[37] are so close to the unperturbed lifetime of the coumarin dye in solution that they almost certainly originate from the dye that was not bound to the semiconductor. In contrast, single molecule emission lifetime experiments on the cresyl violet dye on a continuous indium tin oxide glass surface revealed a much more pronounced quenching and a very broad distribution of quenching rates, with a sharp cutoff at 100 ps determined by the time resolution of the TCSPC system.[38]

Conclusions

We conclude that the bulk of the residual emission that can be detected from sensitized TiO_2 mesoporous films originates from dye molecules that are trapped within the channels of the film rather than those covalently attached to the surfaces of the semiconductor nanoparticles. It is likely that the wide range of emission lifetimes reflects the distribution of mean free paths experienced by the loose dye molecules diffusing within the porous, spongelike TiO_2 film prior to encountering a nanoparticle and undergoing oxidative quenching. The intensity of the residual emission from individual nanoparticles from which the loose dye was removed by extensive dialysis is orders of magnitude lower. This shows that the common practice of rinsing the sensitized films falls well short of removing all unbound and physisorbed dye. The high absorption cross-sections of sensitized films, which were in some instances explained in terms of difficult to quantify parameters such as the surface roughness factor and the fractal nature[13] of the TiO_2 films are much more likely the result of such interstitial trapping and formation of multiple physisorbed layers of the dye. The emission lifetimes obtained from the dialyzed sensitized nanoparticles are much shorter, with the dominant components on sub-nanosecond and short nanosecond time scales. We believe that these excited-state lifetimes, which are still surprisingly long in comparison with the results of the pump−probe experiments, originate from dye molecules bound to surface defects. These results also emphasize the importance of simultaneous spectral and temporal characterization of the dye-modified nanoparticles as some of the residual emission may originate from impurities in the substrate and the decomposition products, which cannot be distinguished on the basis of the quenching dynamics alone. Last, it should be noted that identifying a representative dye molecule in true "single molecule−single nanoparticle" experiments is a very challenging task due to a heavy bias toward dye molecules that undergo anomalously slow injection.

Acknowledgment. The support of this work by the National Science Foundation Nanoscale Interdisciplinary Research Grant (No. 0303829) and a National Science Foundation Chemical Instrumentation Grant (No. 0342432) is gratefully acknowledged. Support from the FWO, the Flemish Ministry of Education (Grant No. GOA 2001/02), the BMBF, the Federal Science Policy of Belgium (Grant No. IAP-V-03), a Max Planck research award, and the Eurocores grant (Bionics) is also acknowledged. We thank the group of Professor Huixin He for the atomic force microscopy images of TiO_2 films and nanoparticles.

References and Notes

(1) Burfeindt, B.; Hannappel, T.; Storck, W.; Willig, F. *J. Phys. Chem.* **1996**, *100*, 16463−16465.

(2) Hannappel, T.; Burfeindt, B.; Storck, W.; Willig, F. *J. Phys. Chem. B* **1997**, *101*, 6799−6802.

(3) Benko, G.; Kallioinen, J.; Korppi-Tommola, J. E. I.; Yartsev, A. P.; Sundstrom, V. *J. Am. Chem. Soc.* **2002**, *124*, 489−493.

(4) Kallioinen, J.; Benko, G.; Sundstrom, V.; Korppi-Tommola, J. E. I.; Yartsev, A. P. *J. Phys. Chem. B* **2002**, *106*, 4396−4404.

(5) Benko, G.; Skarman, B.; Wallenberg, R.; Hagfeldt, A.; Sundstrom, V.; Yartsev, A. P. *J. Phys. Chem. B* **2003**, *107*, 1370−1375.

(6) Kallioinen, J.; Benko, G.; Myllyperkio, P.; Khriachtchev, L.; Skarman, B.; Wallenberg, R.; Tuomikoski, M.; Korppi-Tommola, J.; Sundstrom, V.; Yartsev, A. P. *J. Phys. Chem. B* **2004**, *108*, 6365−6373.

(7) Kuciauskas, D.; Monat, J. E.; Villahermosa, R.; Gray, H. B.; Lewis, N. S.; McCusker, J. K. *J. Phys. Chem. B* **2002**, *106*, 9347−9358.

(8) Huber, R.; Moser, J.-E.; Gratzel, M.; Wachtveitl, J. *J. Phys. Chem. B* **2002**, *106*, 6494−6499.

(9) Rehm, J. M.; McLendon, G. L.; Nagasawa, Y.; Yoshihara, K.; Moser, J.; Gratzel, M. *J. Phys. Chem.* **1996**, *100*, 9577−9578.

(10) Piotrowiak, P.; Galoppini, E.; Wei, Q.; Meyer, G. J.; Wiewior, P. *J. Am. Chem. Soc.* **2003**, *125*, 5278−5279.

(11) Martini, I.; Hodak, J. H.; Hartland, G. V. J. *Phys. Chem. B* **1998**, *102*, 9508−9517.

(12) Martini, I.; Hodak, J. H.; Hartland, G. V. *J. Phys. Chem. B* **1998**, *102*, 607−614.

(13) Martini, I.; Hodak, J. H.; Hartland, G. V. *J. Phys. Chem. B* **1999**, *103*, 9104−9111.

(14) Asbury, J. B.; Ellingson, R. J.; Ghosh, H. N.; Ferrere, S.; Nozik, A. J.; Lian, T. *J. Phys. Chem. B* **1999**, *103*, 3110−3119.

(15) Ghosh, H. N.; Asbury, J. B.; Lian, T. *J. Phys. Chem. B* **1998**, *102*, 6482−6486.

(16) Asbury, J. B.; Hao, E.; Wang, Y.; Lian, T. *J. Phys. Chem. B* **2000**, *104*, 11957−11964.

(17) Ghosh, H. N.; Asbury, J. B.; Weng, Y.; Lian, T. *J. Phys. Chem. B* **1998**, *102*, 10208−10215.

(18) Kilsa, K.; Mayo, E. I.; Kuciauskas, D.; Villahermosa, R.; Lewis, N. S.; Winkler, J. R.; Gray, H. B. *J. Phys. Chem. A* **2003**, *107*, 3379−3383.

(19) Desilvestro, J.; Graetzel, M.; Kavan, L.; Moser, J.; Augustynski, J. *J. Am. Chem. Soc.* **1985**, *107*, 2988−2990.

(20) Vlachopoulos, N.; Liska, P.; Augustynski, J.; Graetzel. M. *J. Am. Chem. Soc.* **1988**, *110*, 1216−1220.

(21) Hashimoto, K.; Hiramoto, M.; Lever, A. B. P.; Sakata, T. *J. Phys. Chem.* **1988**, *92*, 1016.

(22) Argazzi, R.; Bignozzi, C. A.; Heilmer, T. A.; Castellano, F. N.; Meyer, G. J. *Inorg. Chem.* **1994**, *33*, 5741.

(23) Ford, W. E.; Rodgers, M. A. J. *J. Phys. Chem.* **1994**, *98*, 3822.

(24) Bedja, I.; Hotchandani, S.; Kamat, P. V. *J. Phys. Chem.* **1994**, *98*, 4133.

(25) Vinodgopal, K.; Hua, X.; Dahlgren, R. L.; Lappin, A. G.; Patterson, L. K.; Kamat, P. V. *J. Phys. Chem.* **1995**, *99*, 10883−10889.

(26) Fessenden, R. W.; Kamat, P. V. *J. Phys. Chem.* **1995**, *99*, 12902−12906.

(27) Fessenden, R. W.; Kamat, P. V. *Chem. Phys. Lett.* **1986**, *123*, 233.

(28) Eichberger, R.; Willig, F. *Chem. Phys.* **1990**, *141*, 159.

(29) O'Regan, B.; Moser, J.; Anderson, M.; Graetzel, M. *J. Phys. Chem.* **1990**, *94*, 8720−8726.

(30) Cotlet, M.; Hofkens, J.; Maus, M.; De Schryver, F. C. In *Fluorescence Spectroscopy, Imaging and Probes: New Tools in Chemical, Physical, and Life Sciences*; Kraayenhof, R.; Visser, A. J. W. G.; Gerittsen, H. C., Eds.; Springer: Berlin, 2002; pp 181−224.

(31) Maus, M.; Cotlet, M.; Hofkens, J.; Gensch, T.; De Schryver, F. C.; Schaffer, J.; Seidel, C. A. M. *Anal. Chem.* **2001**, *73*, 2078−2086.

(32) Heimer, T. A.; Heilwel, E. J. *J. Phys. Chem. B* **1997**, *101*, 10990−10993.

(33) Umpathy, S.; Carther, A. M.; Parker, A. W.; Hester, R. E. *J. Phys. Chem.* **1990**, *94*, 1357.

(34) Qu, P.; Thompson, D. W.; Meyer, G. J. *Langmuir* **2000**, *16*, 4662−4671.

(35) Shimizu, O.; Watanabe, J.; Naito, S. *Chem. Phys. Lett.* **2000**, *332*, 295.

(36) van't Spijker, H.; Goossens, A. *Thin Solid Films* **2002**, *403−404*, 410−414.

(37) Biju, V.; Micic, M.; Hu, D.; Lu, H. P. *J. Am. Chem. Soc.* **2004**, 126, 9374−9381.

(38) Lu, H. P.; Xie, X. S. *J. Phys. Chem. B* **1997**, *101*, 2753−2757.

(39) Wang, H. Z.; Zhao, F. L.; He, Y. J.; Zheng, X. G.; Huang, X. G.; Wu, M. M. *Opt. Lett.* **1998**, *23*, 777−779.

(40) Popp, J.; Fields, M. H.; Chang, R. K. *Opt. Lett.* **1997**, *22*, 139−141.

(41) Lin, H.-B.; Eversole, J. D.; Campillo, A. J.; Barton, J. P. *Opt. Lett.* **1998**, *23*, 1921−1923.

(42) Popp, J.; Fields, M. H.; Chang, R. K. *Opt. Lett.* **1997**, *22*, 1296−1298.

(43) Borchers, M. A.; Esen, C.; Schweiger, G. *Opt. Lett.* **2001**, *26*, 346−348.